Acta Mech 228, 2751–2758 (2017)
DOI 10.1007/s00707-015-1523-z

ORIGINAL PAPER

Tsunehisa Miki · Rumiko Nakaya · Masako Seki · Soichi Tanaka · Nobuo Sobue · Ichinori Shigematsu · Kozo Kanayama

Large deformability derived from a cell–cell slip mechanism in intercellular regions of solid wood

Received: 13 April 2015 / Revised: 4 July 2015 / Published online: 17 December 2015

Abstract A uniaxial compression experiment with solid wood under various saturated vapor temperature conditions revealed that remarkable deformation occurred in the tangential direction at higher temperatures of up to 180 °C, with minimal longitudinal deformation. The maximum deformation ratio in the tangential direction exceeded 200 % of the initial specimen diameter although a decrease in thickness became less than the tenth part of the initial one. Microscopic observations indicated that the large deformation behavior resulted from an accumulation of changing original position in mutual wood cells, which led to slip at the intercellular layer. Scanning probe microscopy indicated that this phenomenon was a result of the hierarchical structure of the wood cell and that the intercellular layer becomes selectively softened under specific hygrothermal conditions.

1 Introduction

Wood is a natural polymer composite consisting of cellulose, hemicellulose, and lignin. These chemical components create the multilayered tubular architecture of the wood cell, and crystalline cellulose fibrils at the appropriate angle for the stem direction are embedded in the hemicellulose and lignin of each layer [1]. The wood cells are bonded to each other by the outer layer and middle lamella, where, compared to the other layers, a relatively large amount of matrix substances such as hemicellulose and lignin are contained within the less oriented cellulose. Due to the cellulose fiber-reinforced structure, wood has a higher strength and rigidity along the longitudinal (L) direction of the wood cells. On the other hand, wood is easily deformed and collapsed as densifying the tubular cell structure in the radial (R) and tangential (T) directions perpendicular to the L direction of wood. Due to the complicated hierarchical structure, solid wood, which is an aggregate of wood cells, is generally difficult to plastically deform under an applied stress. Therefore, the present deformation of solid wood was performed by collapsing the hollow tubular cells, which leads to buckling of the cell walls [2]. This means that enlarging deformation, which involves both elongation and expansion, is rarely observed in the densification of solid wood.

In this study, a large elongational deformation in the T direction of solid wood, in which slipping phenomena among mutual wood cells occurred similarly to plastic deformation by slip bands in metallic materials, was observed under uniaxial compression along the R direction under hydrothermal conditions [3–5]. The thermal softening behavior and dimensional changes of wood cells and middle lamellae at elevated temperatures were

T. Miki (✉) · R. Nakaya · M. Seki · N. Sobue · I. Shigematsu
National Institute of Advanced Industrial Science and Technology (AIST), Nagoya 463-8560, Japan
E-mail: tsune-miki@aist.go.jp

S. Tanaka · K. Kanayama
Kyoto University, Kyoto, Japan

investigated using scanning probe microscopy (SPM) under hygrothermal conditions. Finally, the role of the cell–cell slip mechanism in the large deformation is discussed.

2 Experimental procedure

2.1 Wood specimens

Coniferous Hinoki (*Chamaecyparis obtusa*) sapwood specimens were used in this experiment. Longitudinally continuous specimens were prepared with a round shape 5 mm in diameter (L–T directions) and 3.5 mm high (R direction) from plain-sawn lumber (bulk density in dry air: 0.37 g/cm^3, average annual ring width: 0.5 mm) using a computer-controlled milling cutter (Egx-20 Roland DG Co., Ltd.). The moisture content of all specimens was adjusted to 200 %, which is based on the dry mass of wood, by degassing for one hour and soaking in water for one day.

For hygrothermal SPM observations, 40-μm-thick sliced specimens (R–T directions) were prepared using a freezing microtome method. The specimens were dried gently at room temperature between glass slides after being conditioned in water to avoid inducing curvature or splitting by rapid drying.

2.2 Compressing in saturated vapor conditions

A uniaxial compression test was carried out using a material testing machine equipped with a pressure container made by Yonekura Mfg. Co., Ltd. (CATY TC-2kN-NS), as schematically illustrated in Fig. 1. The testing machine enabled horizontal compression tests of the water-saturated wood in confined heating conditions with water above 100 °C while recording load–stroke curves during hydrothermal compression. The compression temperature T_v was set from a temperature at the saturated vapor pressure, which is equivalent to the pressure in a hermetically sealed container where water at a pit is heated by cartridge heaters. Sliding resistance load between heatproof rubber packings and rams derived from sealing during movements of the rams was measured and subtracted out before each compression test at a given specimen temperature.

In the initial setup for the compression test, the specimen was held between cylinders by a force of 2–3 N, and heating was carried out by heating the water after closing the container. Five minutes after the thermocouple indicated that the target temperature had been achieved, the compression test was conducted at a compression speed of 1 mm/min up to a maximum compressive load of 2000 N.

2.3 Observations

To understand the deformation behavior of the wood specimens, changes in the diameter, height, and surface were observed using a digital microscope (Keyence VHX-900). Interior structural changes were also observed by scanning electron microscope (SEM) after a thin Au layer coating was applied over the cut surface.

Scanning probe microscopy (SPM), atomic force microscopy (AFM), and nanoindentation are useful tools for the characterization of wood structures at the nanoscale [6–9]. To investigate the large deformation in more detail, SPM in hygrothermal conditions using an AFM5100N with a heating unit made by Hitachi High-Tech Science Corporation was also performed. Dynamic force mode (DFM) with a sampling intelligent scan mode (SIS) was applied using a pyramidal-tipped silicon cantilever (spring constant $K = 2.1$ N/m, resonance frequency $F = 72$ kHz). To enable SPM observations in both air and water, a 1×1 mm^2 piece of sample was attached to a shallow Al dish with adhesive tape, which did not influence the wood properties. Measurements were taken in both air and water at room temperature and at 50 °C. The scanning period of each measurement required about 10 minutes to acquire sufficient resolution. Force–distance curve measurements around the intercellular regions were also taken to estimate the surface properties involving the hardness and stickiness at a constant speed of 10 nm/s of cantilever movement. The detected deflection of the cantilever was converted to load by the spring constant K.

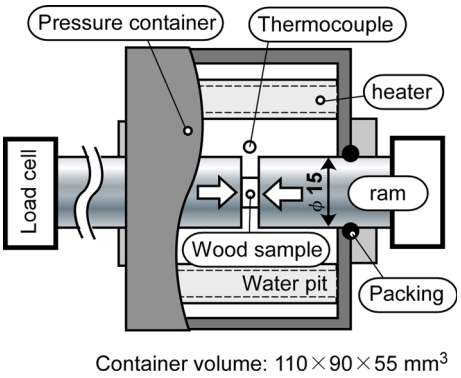

Fig. 1 Schematic drawing of a uniaxial compression test

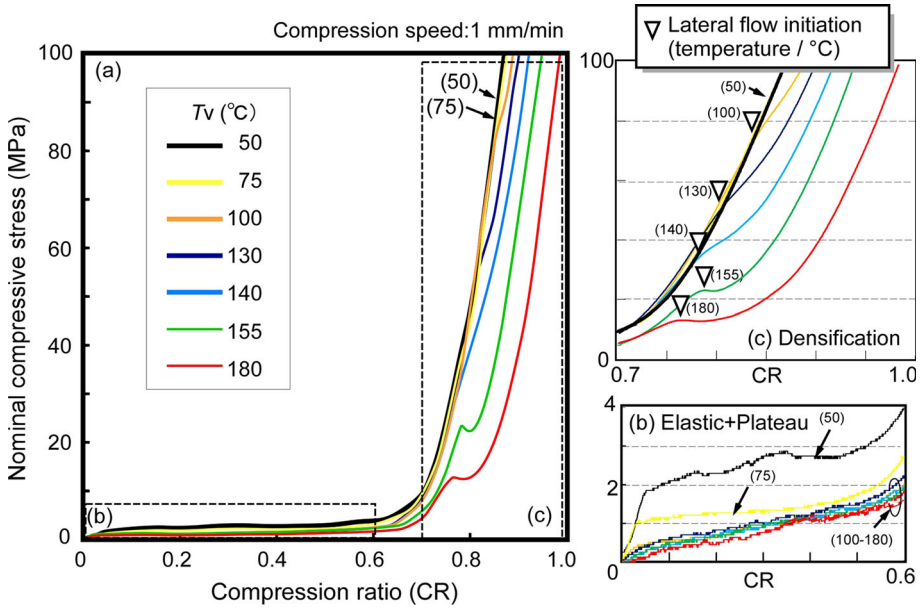

Fig. 2 Compressive stress–compression ratio curves

3 Results and discussion

3.1 Deformation behavior

Figure 2a shows nominal compressive stress and compression ratio curves obtained at various temperatures. The nominal stress was obtained from the detected load divided by the initial cross-sectional area of the wood specimen, and the compression ratio (CR) is the ratio of the stroke divided by the initial specimen height. The true stress applied on the specimen was hard to be obtained because an abrupt increase in the cross-sectional area during pressing was generated. As can be seen in the figure, the wood specimen kept deforming under a relatively low compressive stress up to almost 63 % of the compression ratio, regardless of the temperature. Beyond this stage, the wood specimen underwent an elastic plateau process in which the wood cells collapsed as the cell walls buckled. In the enlarged view of the elastic plateau region (b), the deformation stress determined from the plateau stress drastically decreased at higher compression temperatures up to 100 °C. Above this temperature, the deformation stress decreased slightly. This is due to softening of the wood cells by heat and moisture and is related to the glass transition temperatures of hemicellulose and lignin. Considering that the porosity of the wood specimen, as calculated from the bulk density, was 74 %, the 63 % compression rate almost reached the true density of the wood specimen (1.45 g/cm^3). Above this compression ratio, the compressive stress required to deform the wood specimen rapidly increased with increasing stroke. In this deformation stage, the shape of the compression curve depended upon the compression temperature, as can

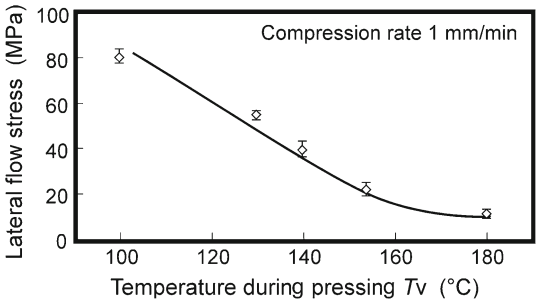

Fig. 3 Effect of compression temperature on the flow stress

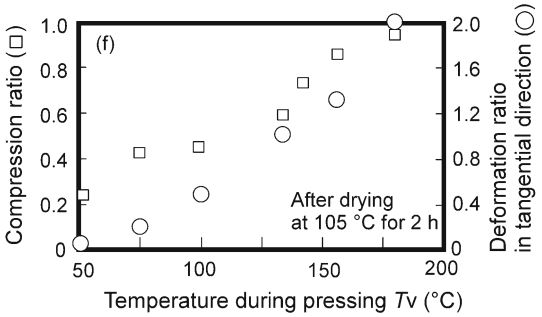

Fig. 4 Effect of compression temperature on deformation ratio and compression ratio

be seen in the enlarged view of the densification process (c). Thus, the deformation behavior of the wood specimen was affected by the compression temperature. As shown in the enlarged view, the compressive stress rose exponentially with increasing stroke up to 75 °C, but there was an inflection point (indicated by inverted triangles) on the compressive stress curve above 100 °C. This inflection point becomes more significant at higher compression temperatures. Until the inflection point, the volume of the lumen decreases as wood cells buckle and densify. This deformation behavior is typically seen in the process of compression or densified woods. Since the wood specimen did not suffer from any lateral restrictions in the present compression tests, it was supposed that lateral deformation and flow would occur above a critical shear stress or during fracture of the specimen. In saturated water conditions, the intercellular regions, such as the area around the middle lamella, become weaker, facilitating the generation of flow deformation among the wood cells. Consequently, the deflection point arises from the initiation of flow deformation behavior. It was found that flow deformation occurred at lower compressive stresses when the temperature was higher, as summarized in Fig. 3. The lateral flow stress decreased up to 150 °C, above which the rate of decrease slowed. Many studies have mentioned a softening behavior in this temperature region that occurs due to the phase transitions of lignin in wood [10,11]. The lateral flow stress was decreased by 25 % by heating to 150 °C.

3.2 Appearance and dimensional changes

Figures 4 and 5 show the dimensional changes of wood specimens after compression testing and the corresponding changes in appearance from top (L–T surface) and side (R–T surface) views, respectively. Spring back along the compression direction (the R direction of the specimen) was observed in all tests. Thus, the compression ratio can indicate the appearance of plastic deformability. The compression ratio drastically increased above 130 °C and exceeded 90 % at 180 °C. The deformation ratio in the T direction, which comes from the maximum elongation in the tangential direction compared to the initial diameter, increased linearly with increasing temperature, exceeding 200 % at 180 °C. There was a strong positive correlation between the compression ratio and the deformation ratio in the tangential direction.

In Fig. 5, the top views of specimens (a) and (b) are similar, although a large buckling arose in the compression at 75 °C, as shown in the side view. Around 100 °C, lateral (tangential) deformation appeared to initiate. Above 130 °C, the lateral deformation increased significantly, along with a remarkable decrease in thickness. The compression in 180 °C of the temperature decreased the thickness of the wood specimen to

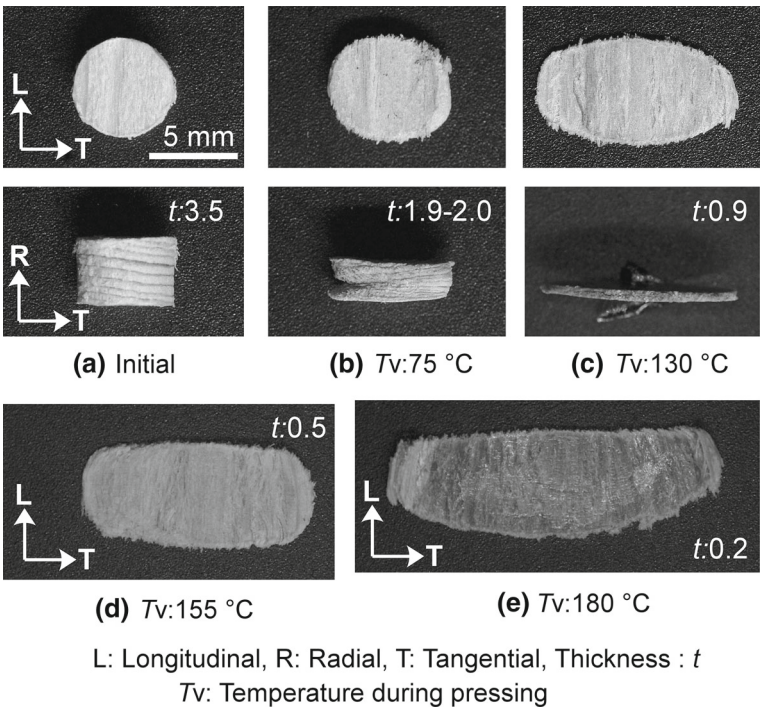

Fig. 5 Appearance of specimens deformed at various temperatures

200 μm from an initial 3.5 mm. In the longitudinal direction, however, very little deformation occurred under the temperature conditions applied in this experiment. This anisotropy in deformability is derived from the naturally constructed rigid cellulose-reinforced structure of the cell wall along the L direction.

3.3 Microstructure changes

Microstructural changes observed by SEM and optical microscopy on the cut surface of wood specimens after compression testing to the following deformation stages: initial (A–B), densification (C–D), and flow (E–F), are shown in Fig. 6. In the figure, broken lines "a," white double-headed arrows "b," and enclosed lines "c" indicate annual rings, ray cells, and tracheid cells, respectively. As shown in A and B, natural wood has neatly arranged tracheid cells (c) in the R direction, and the cell lumen becomes narrower close to the annual ring (a). The size of the tracheid cells ranged from 10 to 20 μm. Between the annual rings, ray cells (b) were present along the R direction. After densification under compression in the R direction, the lumens disappeared as buckling ray and tracheid cells collapsed completely, as shown in C and D, although the annual ring still can be recognized. The tracheid cells seemed to have densified and elongated in the T direction. During flow deformation, as shown in E and F, the cell deformation was more prominent, and the positional relationship between the cells changed partially. As neighboring cells swap positions, the continuity of the annual ring is disrupted. Slip lines are generated roughly 45° from the compression direction (black triangles), and cell–cell slippage occurs along these lines, leading to a large deformation of the solid wood.

3.4 Local property changes

Height and phase images obtained by SPM measurements in both air (dry) and water (wet) are shown in Fig. 7. Images of $18 \times 18\,\mu m^2$ scanned areas of R–T cut surfaces in dry (a) and wet (d) states are shown, where a higher brightness indicates a higher position. In the images, cells (indicated with an *) enclosed by intercellular structures called middle lamella can be recognized. Comparing the dry and wet states, it seems that the swelling of hollow cells by water resulted in closed cavities (**) as well as an increased asperity around the intercellular regions. Enlarged views of the $8 \times 8\,\mu m^2$ scanning areas marked (i) in (a) and (ii) in (d) are represented as

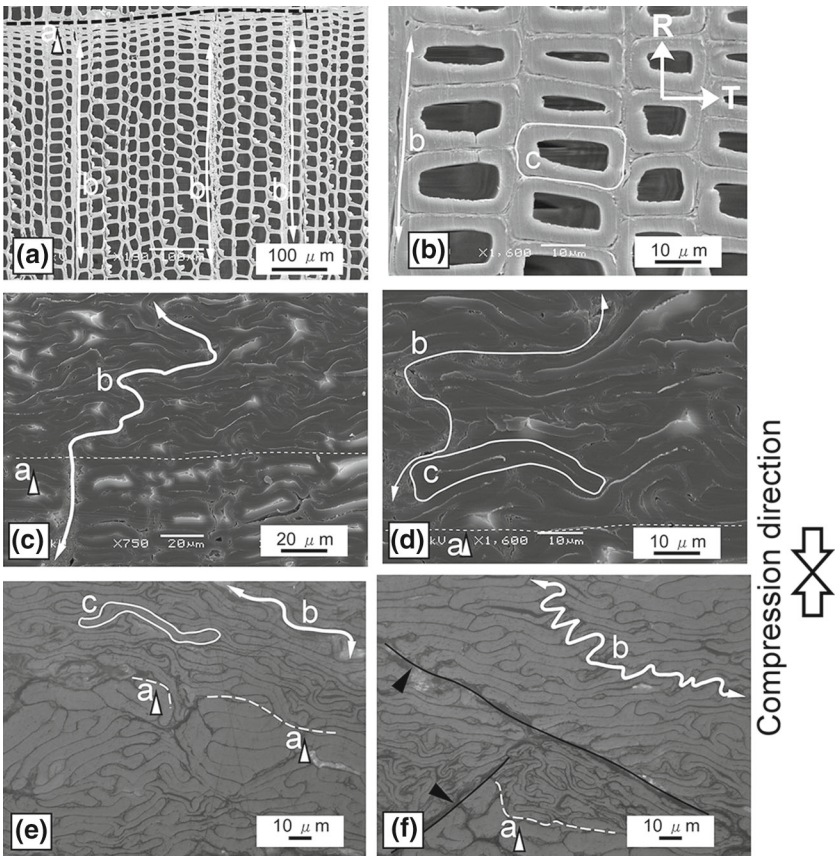

Fig. 6 Microstructure changes of wood after flow deformation

height (b), (e) and phase (c), (f) images. The height images (b) and (e) show cell–cell aggregation connected by middle lamella in an intercellular region. Drastic height and geometry changes occurred with the adsorption of water. The middle lamella became higher and wider than the cells. The height profiles along A–A' in (b) and B–B' in (e) are plotted in Fig. 8a. Clearly, intercellular structures in the wet state swelled to form a plateau above the surrounding material/cells but formed a lower valley-like level in the dry state. An even higher degree of swelling was observed at the boundaries between middle lamellae and cells, indicated with white arrows in the figure. Therefore, in the wet state, the primary wall between a cell (secondary wall) and the intercellular layer would swell more than a layer consisting of only the cell.

Figure 7c, f shows phase images that represent the phase lag of the resonance frequency of the cantilever due to interactions between the cantilever tip and a material surface, such as a variation in adsorption force, hardness, or electrical force. A darker region indicates a greater phase lag. In the wet state, darker regions were observed along the boundary regions of cells, although in the dry state very little phase lag was observed. This indicates that the boundary regions of the cells became softer and stickier than the other portions by adsorbing moisture. To estimate properties involving the softness or stickiness, force curve measurements were taken with the cantilever indented on regions identified as cell, primary wall, or intercellular layer by cantilever movements from −50 to 20 (dry) or 30 (wet) nm. This method obtains a force–distance curve, which can be applied for estimating living cell mechanical properties [12]. Figure 8b shows the results of force–distance curve measurements in dry and wet states, with the numbers corresponding to those in Fig. 7c, f. The slope of the applied load for the cantilever position implies rigidity, and the negative load values obtained in the dry state indicate a sticking force, which show an ability of adsorption between cantilever tip and a material surface. In the dry state, the difference in the rigidity indicated by the slope was almost the same (about 0.17 N/m) for all of the intercellular structures. However, there was a slight increase in the stickiness of the intercellular layer in the dry state. Force–distance curve measurements in the wet state indicated that moisture causes large differences in rigidity for each of the cell structures (secondary wall, primary wall, and intercellular layer). Swollen intercellular structures (numbers 2, 3, and 4) became much softer than the cells (1 and 5). The rigidity

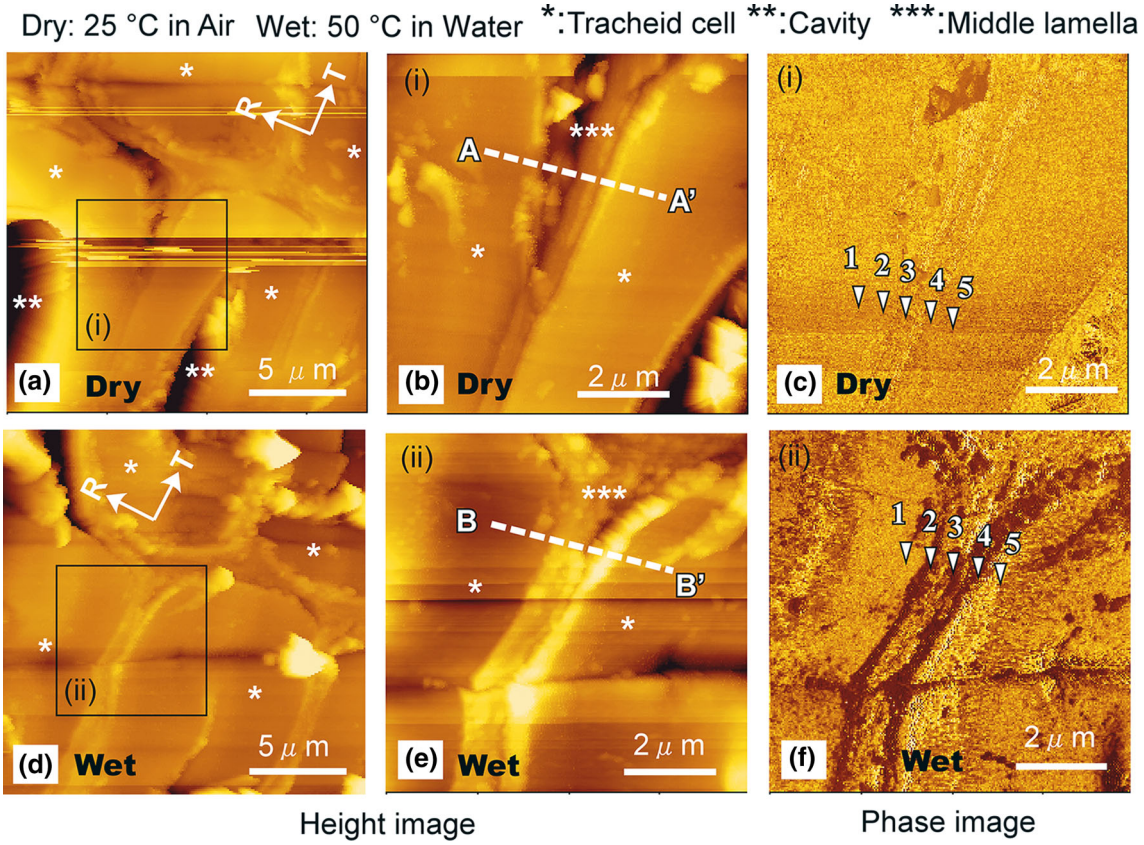

Fig. 7 Scanning probe microscopic images of wood cell aggregates in dry and wet conditions

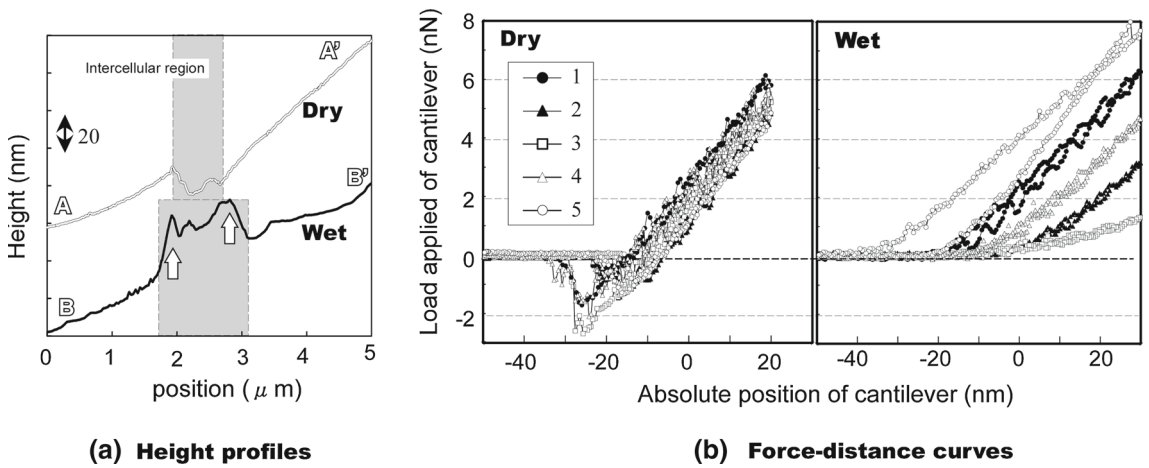

Fig. 8 Local height profiles and force curve variation of wood in dry and wet conditions

of wet cell, primary wall, and intercellular layer were approximately 0.12, 0.09, and 0.02 N/m, respectively. The intercellular layer became very soft after swelling.

Consequently, the primary cell wall swells more in the height (L) direction than the middle lamella. In the phase images, brighter regions indicate more sticky and viscous locations. Thus, the boundary region around the primary cell wall can be selectively softened due to swelling in warm water, although in the dry state the primary wall's properties changed very little as compared to the secondary wall.

4 Conclusions

A large elongational deformability of over 200 % in the tangential direction of solid wood was observed in a compression process during the densification stage of cells. SEM and SPM observations indicated that this behavior arose from a slippage mechanism among wood cells in intercellular regions under hydrothermal and hygrothermal conditions.

Acknowledgments This work was partially supported by the Industrial Technology Research Grant Program in 2011 from the New Energy and Industrial Technology Development Organization (NEDO) of Japan, and by a Grant-in-Aid for Scientific Research (A) (No. 232446129) from the Ministry of Education, Culture, Sports, Science and Technology of Japan.

References

1. Frantzl, P., Weinkamer, R.: Nature's hierarchical materials. Prog. Mater. Sci. **52**, 1263–1334 (2007)
2. Sandberg, D., Haller, P., Navi, P.: Thermo-hydro and thermo-hydro-mechanical wood processing: an opportunity for future environmentally friendly wood products. Wood Mater. Sci. Eng. **8**, 64–88 (2013)
3. Miki, T., Sugimoto, H., Kanayama, K.: Deformation behaviour of natural wood having hierarchical structure under a compression state. MRS Fall Meeting Proceedings: 1304 (2011). doi:10.1557/opl.2011.609 (Online publication)
4. Miki, T., Seki, M., Shigematsu, I., Kanayama, K.: Preparation of three dimensional products using flow deformability of wood treated by small molecular resins. Adv. Mater. Res. **856**, 79–86 (2014)
5. Miki, T., Sugimoto, H., Shigematsu, I., Kanayama, K.: Superplastic deformation of solid wood by slipping cells at sub-micrometre intercellular layers. Int. J. Nanotechnol. **11**, 509–519 (2014)
6. Fahlén, J., Salmén, L.: Pore and matrix distribution in the fiber wall revealed by atomic force microscopy and image analysis. Biomacromolecules **6**, 433–438 (2005)
7. Wimmer, R., Lucas, B.N.: Comparing mechanical properties of secondary wall and cell corner middle lamella in spruce wood. IAWA J. **18**, 77–88 (1997)
8. Gindle, W., Schöberl, T.: The significance of the elastic modulus of wood cell walls obtained from nanoindentation measurements. Compos. A **35**, 1345–1349 (2004)
9. Tze, W.T.Y., Wang, S., Rials, T.G., Pharr, G.M., Kelley, S.S.: Nanoindentation of wood cell walls: continuous stiffness and hardness measurements. Compos. A **38**, 945–953 (2007)
10. Hamdan, S., Dwianto, W., Morooka, T., Norimoto, M.: Softening characteristics of wet wood under quasi static loading. Holzforschung **54**, 557–560 (2005)
11. Placet, V., Passard, J., Perré, P.: Viscoelastic properties of wood across the grain measured under water-saturated conditions up to 135 °C: evidence of thermal degradation. J. Mater. Sci. **43**, 3210–3217 (2008)
12. Harris, A.R., Charras, G.T.: Experimental validation of atomic force microscopy-based cell elasticity measurements. Nanotechnology **22**, 1–10 (2011)